Supporting Information

Hierarchical 3-Dimensional Nickel-Iron Nanosheet Arrays on Carbon Fiber Paper as a Novel Electrode for Non-Enzymatic Glucose Sensing

Palanisamy Kannan,[a,c] Thandavarayan Maiyalagan,[b] Enrico Marsili,[c] Srabanti Ghosh,[d] Joanna Niedziolka-Jönsson, [a]* and Martin Jönsson-Niedziolka [a]**

[a] Institute of Physical Chemistry, Polish Academy of Sciences
44/52 ul. Kasprzaka, 01-224 Warsaw, Poland

[b] School of Chemistry, University of East Anglia
Norwich NR4 7TJ, United Kingdom

[c] Singapore Centre on Environmental Life Sciences Engineering (SCELSE)
Nanyang Technological University, 60 Nanyang Drive, SBS-01N-27, Singapore

[d] Department of Chemical, Biological and Macromolecular Sciences
S. N. Bose National Centre for Basic Sciences
Block-JD, Sector-III, Salt Lake, Kolkata-700098, India

*Corresponding Authors: joaniek@ichf.edu.pl (Joanna Niedziolka-Jönsson); martinj@ichf.edu.pl (Martin Jönsson-Niedziolka). Phone: +4822333433130; Fax: +48223433333. emarsili@ntu.edu.sg (Enrico Marsili). Tel: +65-6592-7895; Fax: +65-6515-6751.

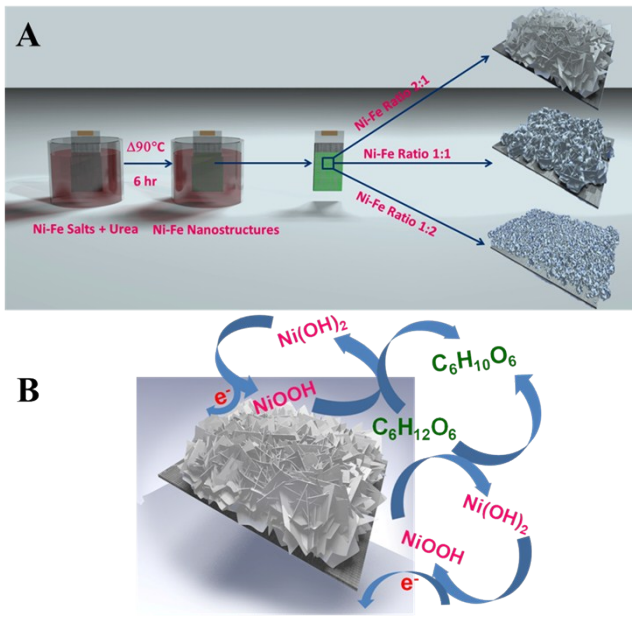

Figure S1. (A) Schematic illustration for the formation of different morphologies of 3-D Ni-Fe hierarchical nanostructures, and (B) the oxidation of glucose molecules on 3-D Ni-Fe hierarchical nanosheet surfaces.

Surface Area Analysis:

Figure S2 depicts the BET nitrogen adsorption and desorption isotherms and pore size distribution of hierarchical Ni-Fe nanostructures. The hysteresis loop appearing in the relative pressure (P/P_0) range of ~0.4–1 indicates the presence of mesopores in the as-prepared samples, which is associated with the mesopore filling and the monolayer coverage of the mesopores. The hierarchical Ni-Fe nanosheets provided a high specific surface area, which was estimated by the Brunauer–Emmett–Teller (BET) method to be 337.9 $m^2\ g^{-1}$, much higher than hierarchical Ni-Fe nanospheres (211.3 $m^2\ g^{-1}$), and porous Ni-Fe nanospheres (136.4 $m^2\ g^{-1}$), respectively. The pore-size distribution plot (inset in Figure S2) shows a bimodal mesopores distribution, whose pore size is ~7.5 nm, obtained by the adsorption branch. This type of porosity would enhance the special surface area, which means hierarchical Ni-Fe nanosheets allows for the rapid access of electrolyte ions, provides abundant active sites for the electrocatalytic reactions, and facilitates fast electron transport between the electrode materials and the analytes. Taking advantage of the flexibility and robustness of CFP, the composite material was fabricated as a flexible biosensor and used as a new type of electrode for the measurement of analytes of interest, e.g., glucose is the case here.

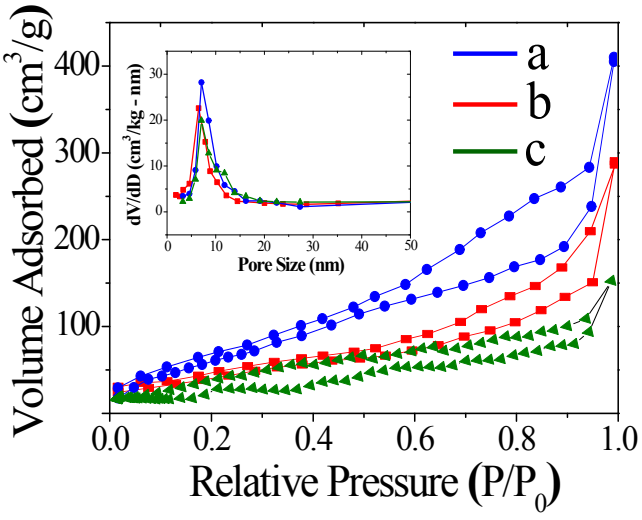

Figure S2. BET nitrogen adsorption and desorption isotherms, and BJH pore size distribution (inset) of 3-D/Ni-Fe hierarchical nanosheets (a), 3-D/Ni-Fe hierarchical nanospheres (b), and 3-D/Ni-Fe porous nanospheres (c) on CFP substrate.

XPS and EDS Analysis:

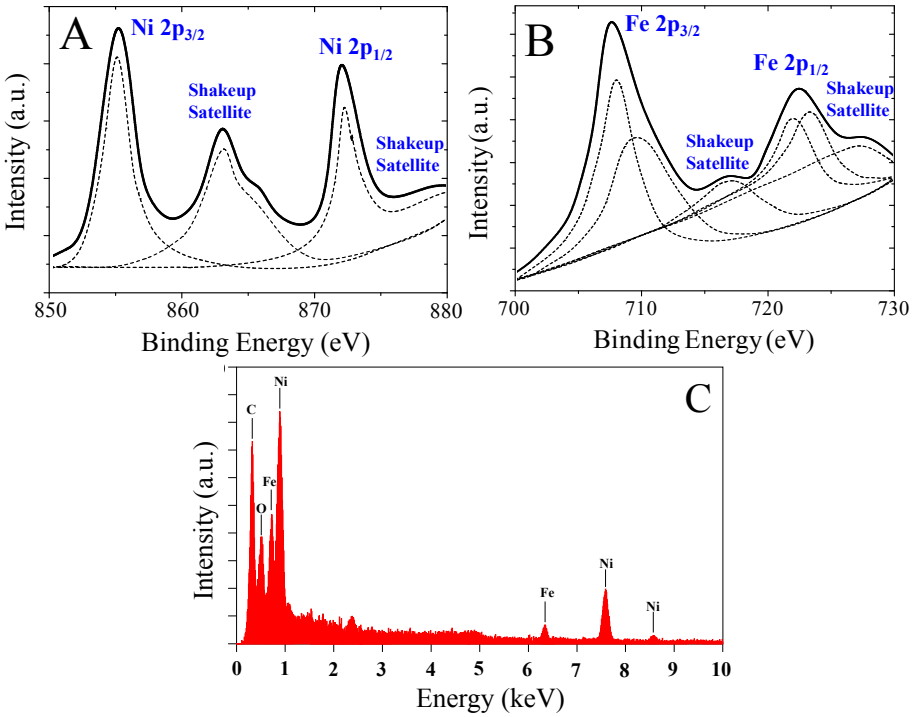

Figure S3. High resolution XPS spectra of Ni 2p (A), and Fe 2p (B) peaks observed in 3D-hierarchical Ni-Fe nanosheets, and its corresponding EDX spectrum (C).

Amperometric Interference Study: One of the major challenges in non-enzymatic glucose analysis is to eliminate the interference responses generated by some endogenous species such as AA, DA, UA, and AP. In the physiological condition, the level of glucose (4.4−6.6 mM) is much higher than that of these species (<0.5 mM). We recorded the amperometric responses of 0.5 μM glucose (steps a, b, g, k, l, and m), 250 μM of AA (step c), DA (step d), UA (step e), AP (step f), fructose (step h), galactose (step i), and lactose (step j) in homogeneously stirred 0.1 M NaOH solution, as shown in Figure S4B. It was found that 3-D/Ni-Fe hierarchical nanosheet arrays provide remarkable responses only for glucose oxidation, and there is no obvious amperometric current response for interfering species as compared to glucose, agreeing well with the Ni based electrodes.[1,2] The long-term stability of the non-enzymatic sensor was evaluated, the CV response of 0.25 mM glucose in 0.1 M NaOH recorded at different time intervals (Figure S4C), we observed no noticeable change in peak potential and peak current towards oxidation of glucose in one day, and a slight decrease (2.8%) in the oxidation current response of glucose was observed for 2 days, and the current decreased by only 8.1% after two weeks. The 3-D/Ni-Fe hierarchical nanosheet arrays CFP electrode was stored at room temperature when not in use. Further, the CVs were recorded for every 10 min interval up to 18 cycles in 0.25 mM glucose in 0.10 M NaOH solution. We observed no noticeable change in the peak potential and peak current for the oxidation of glucose in both sets of experiments. The coefficient of variation was calculated separately for the two sets of experiments and we found that it remained the same (0.61 and 0.67%) in both sets. This shows that the electrode is reproducible, and does not undergo poisoning by the oxidation products, and so can be used for the repeated measurements of glucose detection. The results indicate that the sensor used retains more than 90% of initial sensitivity in continuous tests, suggesting the sensor has favourable long-term stability. This excellent durability of performance mainly results from the robust mechanical stability of 3-D/Ni-Fe nanomaterials. The interconnected wall-like nanostructures with an abundant mesopores and channels protect it from agglomeration, deformation, and collapse for extended period of time under high anodic potential. As a matter of fact, after 40 successive CV measurements of glucose oxidation in 0.1 M NaOH solution, nanostructure still retains the same 3-D hierarchical nanosheet morphology on CFP substrate, as shown in Figure S4D.

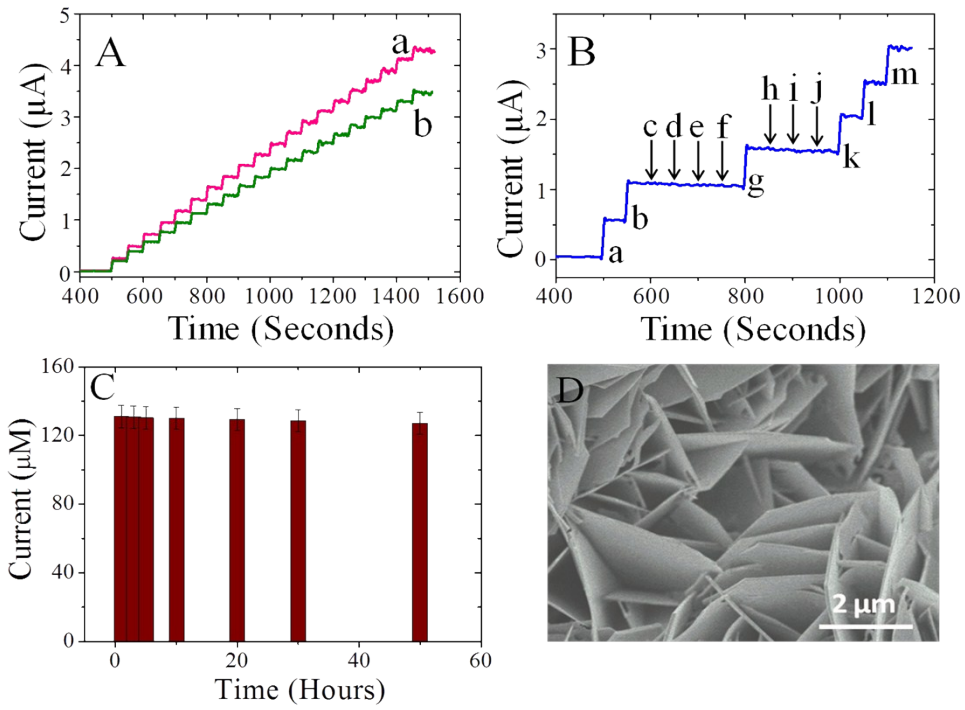

Figure S4. (A) Amperometric response of 3-D/Ni-Fe hierarchical nanospheres, and 3-D/Ni-Fe porous nanospheres CFP electrodes at an applied potential of 0.65 V in constantly stirred 0.1 M NaOH solution with the stepwise addition of 0.5 μM glucose; (B) Amperometric response of 3-D/Ni-Fe hierarchical nanosheet electrode towards the addition of 0.5 μM glucose (a, b, g, k, l, m) and interfering compounds of 250 μM AA (c), DA (d), UA (e), AP (f), fructose (h), galactose (i), and lactose (j) in constantly stirred 0.1 M NaOH solution; (C) Plot of current vs. time for the oxidation of glucose (0.25 mM) at 3-D/Ni-Fe hierarchical nanosheet CFP electrode in 0.1 M NaOH solution, demonstrating the operational stability. The average of two independent measures on different electrodes is reported; (D) FE-SEM measurement was carried out after 40 voltammetric cycles towards the oxidation of glucose (0.25 mM) in 0.1 M NaOH solution.

Table S1. Comparison of the detection limit of the fabricated non-enzymatic glucose sensor based on Ni or Ni-Fe and other metals based nanomaterials.

Nanomaterials modified electrodes	**Detection Limit (μM)**	**References**
Ni nanoparticles decorated titania nanotube arrays	2 μM	1
Ordered Ni nanowires arrays	0.10	2
Honeycomb-like Ni@C	0.90	3
$Ni(OH)_2$ nanoplates/RGO	0.60	4

Dendritic Cu−Ni/TiO_2 film	0.35	5
Pd−Ni/Si nanowires	2.88	6
Ni/Al LDH nanosheet film	5.00	7
Pt/Ni nanowires arrays	1.50	8
3D porous Ni networks	0.07	9
Hexagonal $Ni(OH)_2$ nanosheets	0.34	10
Reduced graphene oxide–$Ni(OH)_2$ composites	20.0	11
Ni/CdS bifunctional Ti@TiO_2 core−shell nanowire	0.35	12
Prickly Ni nanowires	0.10	13
PI/CNT–$Ni(OH)_2$ nanospheres	0.36	14
Pt–NiO nanoplates array/rGO nanocomposites	2.67	15
Ni-coordinated, vertically aligned CNT arrays	30.0	16
$Ni(OH)_2$@Cu dendrite structure	0.24	17
$NiFe_2$/ordered mesoporous carbon nanocomposites	2.70	18
Copper nanoparticles on MWCNT surface	0.50	19
NiOH modified nitrogen incorporated nanodiamonds	1.20	20
rGO/PtNi nanocomposite	1	21
rGO/$Ni(OH)_2$ nanocomposite	0.16	22
ZnO-CuO hierarchical nanocomposites	0.21	23
Hierarchical 3-D/Ni-Fe nanosheet arrays	0.031	This work

Table S2. Comparison between the values obtained in hospital and those obtained by using 3-D/Ni-Fe hierarchical nanosheet arrays CFP electrode for the determination of glucose in human whole blood samples.

Sample numbers	Concentration determined in the hospital (mM)[1]	Concentration determined by our method (mM±SD)[2]	Relative standard deviation (% RSD)[3]
1	5.0	4.87±0.13	2.60
2	5.2	5.04±0.12	3.07
3	5.4	5.24±0.11	2.96
4	5.6	5.44±0.13	2.85
5	5.8	5.65±0.12	2.58

[1] As determined by commercial glucometer in whole blood samples (Johnson & Johnson Medical, Ltd.).

[2] As determined by 3D Ni-Fe hierarchical nanosheets in whole blood samples.

[3] The relative standard deviations (RSD) were calculated from at least four observed values for every sample in order to demonstrate the repeatability.

Table S3. Comparison between the values obtained in hospital and those obtained by using 3-D/Ni-Fe hierarchical nanosheet arrays CFP electrode for the determination of glucose in human whole blood samples.

Sample numbers	Spiked (μM±SD)	Measured (μM±SD)	Relative standard deviation (% RSD)[1]
1	100±0.50	96±0.56	4.10
2	120±0.52	115.5±0.60	3.80
3	140±0.52	135.6±0.58	3.18
4	160±0.51	155±0.55	3.16
5	180±0.52	174.5±0.55	3.09

[1] The relative standard deviations (RSD) were calculated from at least three observed values for every sample in order to demonstrate the repeatability.

References

1. Yu, S.; Peng, X.; Cao, G.; Zhou, M.; Qiao, L.; Yao, J.; He, H., *Electrochim. Acta* 2012**, 76**, 512-517.

2. L. M. Lu, L. Zhang, F. L. Qu, H. X. Lu, X. B. Zhang, Z. S. Wu, S. Y. Huan, Q. A. Wang, G. L. Shen, R. Q. Yu, *Biosens. Bioelectron*. 2009, **25**, 218-223.

3. Y. H. Ni, L. N. Jin, L. Zhang, J. M. Hong, *J. Mater. Chem*. 2010, **20**, 6430-6436.

4. Y. Zhang, F. G. Xu, Y. J. Sun, Y. Shi, Z. W. Wen, Z. Li, *J. Mater. Chem*. 2011, **21**, 16949-16954.

5. S. F. Tong, Y. H. Xu, Z. X. Zhang, W. B. Song, *J. Phys. Chem. C* 2010, **114**, 20925-20931.

6. S. C. Hui, J. Zhang, X. J. Chen, H. H. Xu, D. F. Ma, Y. L. Liu, B. R. Tao, *Sens. Actuators B* 2011, **155**, 592-597.

7. X. Li, J. P. Liu, X. X. Ji, J. Jiang, R. M. Ding, Y. Y. Hu, A. Z. Hu, X. T. Huang, *Sens. Actuator B* 2010, **147**, 241-247.

8. S. S. Mahshid, S. Mahshid, A. Dolati, M. Ghorbani, L. X. Yang, S. L. Luo, Q. Y. Cai, *Electrochim. Acta* 2011, **58**, 551-555.

9. X. Niu, M. Lan, H. Zhao, and C. Chen, *Anal. Chem*. 2013, **85**, 3561-3569.

10. B. Zhan, C. Liu, H. Chen, H. Shi, L. Wang, P. Chen, W. Huang and X. Dong, *Nanoscale*, 2014, **6**, 7424-7429.

11. P. Subramanian, J. Niedziolka-Jonsson, A. Lesniewski, Q. Wang, M. Li, R. Boukherroubb and S. Szunerits, *J. Mater. Chem. A*, 2014, **2**, 5525-5533.

12. C. Guo, H. Huo, X. Han, C. Xu, and H. Li, *Anal. Chem*. 2014, **86**, 876-883.

13. R. K. Shervedani, M. Karevan, A. Amini, *Sens. and Actuators Section B*: 2014, **204**, 783-790.

14. Y. Jiang, S. Yu, J. Li, L. Jia, C. Wang, *Carbon* 2013, **63**, 367-375.

15. L. Wang, X. Lu, C. Wen, Y. Xie, L. Miao, S. Chen, H. Li, P. Li and Y. Song, *J. Mater. Chem. A*, 2015, **3**, 608-616.

16. W.-S. Kim, G.-J. Lee, J.-H. Ryu, K. Park, and H.-K. Park, *RSC Adv*., 2014, **4**, 48310-48316.

17. H. Jung, S. H. Lee, J. Yang, M. Cho and Y. Lee, *RSC Adv*., 2014, **4**, 47714-47720.

18. D. Xianga, L Yinb, J. Ma, E. Guo, Q. Li, Z. Li, K. Liu, *Analyst*, 2015,**140**, 644-653.

19. H-X. Wu, W-M. Cao, Y. Li, G. Liu, Y. Wen, H-F. Yang, S-P. Yang, *Electrochim. Acta* 2010, **55**, 3734-3740.

20. C-Y. Ko, J-H. Huang, S. Raina and W. P. Kang, *Analyst* 2013, **138**, 3201-3208.

21. B. Yuan, C. Xu, D. Deng, Y. Xing, L. Liu, H. Pang, D. Zhang, *Electrochim. Acta*, 2013, **88**, 708-712.

22. Y. Mu, D. Jia, Y. He, Y. Mia and H.-L. Wu, *Biosens. Bioelectron.* 2011, **26**, 2948-2952.

23. C. Zhou, L Xu, J. Song, R. Xing, S. Xu, D. Liu, H. Song, *Sci. Rep*. 2014, 7382.